Chinese Chemical Letters 36 (2025) 109846

Contents lists available at ScienceDirect

Chinese Chemical Letters

journal homepage: www.elsevier.com/locate/cclet

Nutrients deprivation of biomimetic nanozymes for cascade catalysis triggered and oxidative damage induced tumor eradication

Yingtao Zhong, Ziwen Qiu, Yanmei Li, Jiaqi Huang, Zhenming Lu, Renjiang Kong, Ni Yan, Hong Cheng*

School of Biomedical Engineering & Guangdong Provincial Key Laboratory of Construction and Detection in Tissue Engineering, Southern Medical University, Guangzhou 510515, China

ARTICLE INFO

Article history:
Received 25 February 2024
Revised 25 March 2024
Accepted 31 March 2024
Available online 1 April 2024

Keywords:
Biomimetic nanozymes
Cascade catalysis
Nutrients deprivation
Starvation therapy
Oxidative damage

ABSTRACT

Deprivation of glucose and lactate provides an effective pathway to terminate the nutrients supplement for tumor growth. In this work, biomimetic nanozymes called m@BGLC are constructed for catalytic tumor inhibition through nutrients deprivation and oxidative damage induction. Concretely, the catalytic enzymes of glucose oxidase (GOx), lactate oxidase (LOx) and chloroperoxidase (CPO) are precrosslinked with bovine serum albumin (BSA) to construct nanozymes, which are then biomimetic functionalized with cancer cell membrane to prepare m@BGLC. Benefiting from the biomimetic camouflage with homologous cell membrane, m@BGLC inherit homotypic binding and immune escape abilities, facilitating the tumor targeting accumulation and preferable cell internalization for improved drug delivery efficiency. Subsequently, under the cascade catalysis of nanozymes, m@BGLC consume glucose and lactate for tumor starvation therapy through nutrients deprivation, and meanwhile, the resulting hyprochloric acid (HClO) causes an oxidative damage of cells to synergistically inhibit tumor growth. *In vitro* and *in vivo* findings demonstrate a robust tumor eradication effect of m@BGLC without obvious adverse reactions *via* the targeted combination therapy. Such cascade catalytic nanomedicine may inspire the development of sophisticated strategies for tumor combination therapy under unfavorable tumor microenvironments.

Tumor cells are characterized with high energy metabolism to maintain fast cell proliferation and resist cell death. In 1926, Otto Warburg discovered that tumor cells consumed glucose as the primary energy source even in the presence of oxygen, which could produce large amounts of lactate [1]. Of note, the glycolysis product of lactate was the secondary cellular metabolic waste, which would be utilized to support tumor growth during glucose deficiency [2–4]. Several neoplasms are featured with glycolysis, and both glucose and lactate play critical roles in sustaining progressive tumor cell proliferation. Moreover, the massive production of lactate would induce the acidification of tumor microenvironment, resulting in tumor metastasis, angiogenesis, immunosuppression and poor therapeutic outcome [5–7]. Therefore, shutting down the nutrient sources of glucose and lactate in tumor cells shows a great potential to restrain the tumor growth by starvation therapy. Better yet, lactate exhaustion could not only normalize tumor microenvironment, but also possess unique advantages to reverse therapeutic resistance [8].

Traditionally, the blockade of glucose transporter 1 (GLUT1) and monocarboxilate transporters (MCTs) could modulate the transportation of glucose and lactate [9,10]. However, a high concentration of inhibitors was demanded for it, and the blocking effect would be quickly terminated owing to the drug excretion. Therefore, a sustained and continuous strategy should be developed to meet the demands for nutrient deprivation and tumor suppression [11]. Recently, catalytic nanomedicine was proposed to consume the glucose or lactate under physiological condition, indicating moderate tumor suppression effects [12–15]. Among which, glucose oxidase (GOx) could efficiently convert glucose into gluconic acid and hydrogen peroxide (H_2O_2), and lactate oxidase (LOx) could catalyze elimination of lactate to produce pyruvate and H_2O_2 [16–18]. Notably, the consumption of glucose and lactate would improve the immunosuppression by regulating programmed cell death ligand-1 (PD-L1) and regulatory T cells (Tregs), contributing to the immune activation for tumor therapy. Even so, nutrient deprivation alone may be not effective enough to inhibit tumor growth given the multiple energy sources of tumor cells [19–21]. Interestingly, H_2O_2 as the major catalytic product of GOx and LOx inspires the utilization of chloroperoxidase (CPO) and H_2O_2 to syn-

* Corresponding author.
E-mail address: chengh@smu.edu.cn (H. Cheng).

https://doi.org/10.1016/j.cclet.2024.109846
1001-8417/

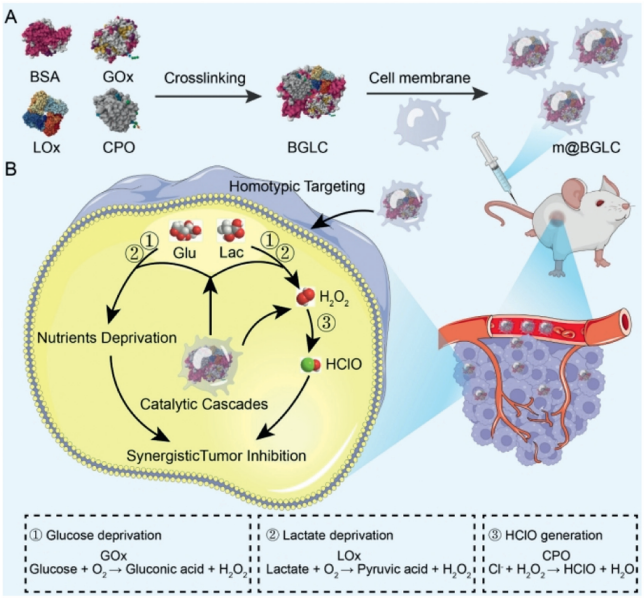

Scheme 1. Schematic illustrations of biomimetic nanozymes (m@BGLC) for tumor treatment. (A) Synthesis process of m@BGLC. (B) The proposed mechanism of m@BGLC for synergistic tumor therapy. After intravenous injection, m@BGLC selectively accumulated at homologous tumor tissues to consume glucose and lactate for starvation therapy through nutrients deprivation. Furthermore, m@BGLC could catalyze the resulting H_2O_2 to generate HClO for inducing oxidative damage. Finally, m@BGLC mediated cascade catalysis enhanced the synergistic tumor therapy.

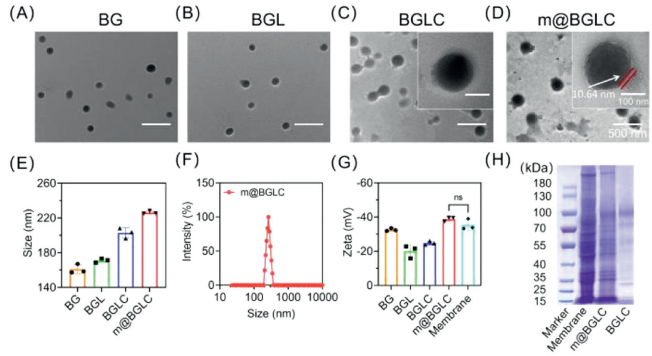

Fig. 1. Characterization of m@BGLC. TEM images of (A) BG, (B) BGL, (C) BGLC, and (D) m@BGLC. Scale bar: 500 nm. (E) Changes of different nanozymes in hydrodynamic diameter ($n = 3$). (F) Hydrodynamic diameter of m@BGLC. (G) Changes of different nanozymes in zeta potential ($n = 3$). (H) SDS-PAGE analysis of m@BGLC. Data are expressed as the mean ± SD.

thesize hypochloric acid (HClO) *in situ* for adjuvant oxidative therapy of tumors [22–24]. Nevertheless, it is challenging to integrate GOx, LOx and CPO into one system with high catalytic efficiency, and the inevitable side effects should be also taken into account because of their poor tumor targeting ability [25–27].

Cancer cells possess some inherent characteristics like cell adhesion and immune escape, which are closely associated with the recognition of cell membrane proteins [28–30]. Recently, the biomimetic strategy of cell membrane functionalization exhibits biomimetic strategy of cell membrane functionalization exhibits superior advantages for homotypic tumor targeting delivery, which could dramatically improve the blood circulation of drugs and reduce undesirable side effects [31–33]. Taking above considerations into account, in this work, biomimetic nanozymes were constructed for catalytic tumor inhibition by nutrients deprivation and inducing oxidative damage. The catalytic enzymes of GOx, LOx and CPO were crosslinked with bovine serum albumin (BSA) to obtain nanozymes called BGLC (Scheme 1A). Subsequently, the breast cancer cell membrane was used for biomimetic modification of BGLC to prepare biomimetic nanozymes (designated as m@BGLC), which preferred to selectively accumulate at homologous tumor tissues for specific cellular uptake. Importantly, the cascade catalytic features of m@BGLC would consume glucose and lactate for tumor starvation therapy through nutrients deprivation (Scheme 1B). Simultaneously, the generated HClO would induce an oxidative damage to synergistically inhibit tumor growth. This design of biomimetic nanozymes with cascade catalytic property might shed light on exploiting bio-derived drug delivery systems for combination therapy of tumor under complex microenvironments.

In this paper, we utilized a naturally occurring polymer BSA to crosslink with the catalytic enzymes, getting biocompatible nanozymes with cascade catalytic property. In which, the amount of feedstock was adjusted to optimize the preparation of BGLC by measuring the catalytic activity and particle size of nanozymes (Fig. S1 in Supporting information). To further increase the specificity to tumor, the nanozymes were coated with 4T1 cell membrane to gain homologous targeting and immune escape abilities for the purpose of biomimetic camouflage. As shown in Figs. 1A–C, the nanozymes with different compositions were prepared as the controls, which showed uniform size and favorable dispersibility. Using the similar methods, BG was prepared based on BSA and GOx. BGL was prepared based on BSA, GOx and LOx. While BGLC was prepared based on BSA, GOx, LOx and CPO. Importantly, transmission electron microscope (TEM) images indicated that m@BGLC were surrounded by cell membranes with the thickness of about 10.64 nm (Fig. 1D). Understandably, an increasing size was found with the addition of further components (Fig. 1E). Among which, the final product of m@BGLC exhibited a narrow nanosize distribution (Fig. 1F), suggesting a good homogeneity of nanoparticles. Afterward, the zeta potentials of BG, BGL and BGLC were measured to be negative, which could be explained by the residual carboxyl groups on the nanozymes (Fig. 1G). Moreover, the zeta potential of BGLC was decreased from −24.80 mV to −38.83 mV following cell membrane coating, which might be attributed to cell membrane surface charge. Additionally, m@BGLC had no significant difference with 4T1 cell membrane in zeta potential value, implying the successful camouflage of nanozymes by biological membrane. Subsequently, sodium dodecyl sulfate-polyacrylamide gel electrophoresis (SDS-PAGE) analysis demonstrated that the protein bands of m@BGLC matched those of 4T1 cell membrane, showing a well reservation of membrane proteins on biomimetic nanozymes, which is required for efficient homologous targeting and immune escape (Fig. 1H). Meanwhile, the diameter and polydispersity (PDI) of m@BGLC in diverse media fluctuated only slightly over 14 days, demonstrating that m@BGLC had feasible stability in physiological conditions (Fig. S2 in Supporting information).

To explore the catalytic performance of m@BGLC, the consumption of glucose, lactate and H_2O_2 was measured using commercial assay kits (Fig. S3 in Supporting information). First, as described in Fig. 2A, the nanozymes showed potent glucose-consuming property. Notably, the glucose could be catalyzed by GOx to produce gluconic acid and H_2O_2. Thus, the catalytic efficiency of m@BGLC could be evaluated by measuring the pH value. As seen in Fig. 2B, the glucose solution displayed a considerable pH decrease within 40 min. In addition, it was found that the lactate concentration did not change a lot in the BG group due to the lack of LOx, whereas BGL, BGLC and m@BGLC demonstrated significant lactic acid consumption (Fig. 2C). Even though m@BGLC were slightly less effective than free LOx, it still caused a 34.53% reduction of lactate level, suggesting a considerable lactate catalytic capability. Since LOx and GOx catalyzed glucose and lactic acid with the assistance of oxy-

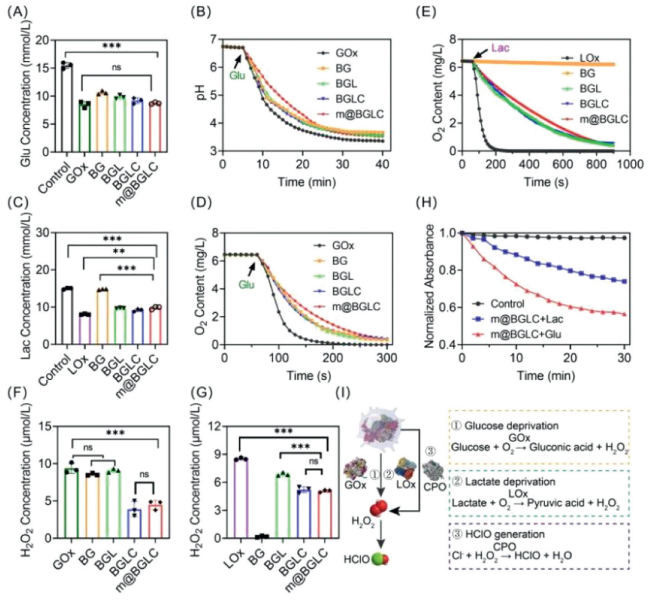

Fig. 2. Evaluation of catalytic performance. (A) Changes of glucose concentration after different treatments with nanozymes ($n = 3$). (B) Nanozymes initiated catalytic changes of the pH value in glucose solution. (C) Changes of lactate concentration after different treatments with nanozymes ($n = 3$). Time-course O_2 consumption of (D) glucose solution and (E) lactate solution after different treatments with nanozymes. Changes of H_2O_2 concentration in (F) glucose solution and (G) lactate solution after different treatments ($n = 3$). (H) The decay curves of MCD absorbance at 290 nm in different groups. (I) Diagram of cascade catalytic mechanism of biomimetic nanozymes. Data are expressed as the mean ± SD. $^{**}P < 0.01$, $^{***}P < 0.001$. ns, no significance; Glu, glucose; Lac, lactic acid.

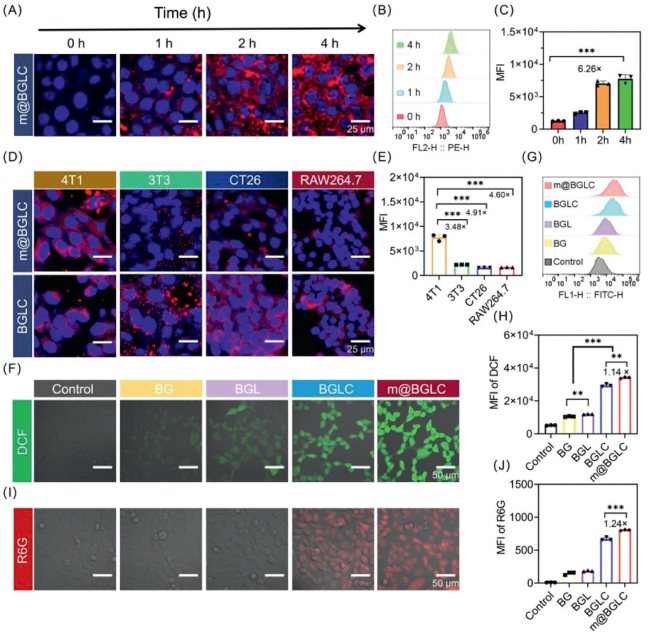

Fig. 3. Cellular uptake and ROS generation of m@BGLC. (A) Intracellular uptake of m@BGLC in 4T1 cells after different incubation time. Scale bar: 25 μm. (B) Flow cytometry histograms and (C) the quantitative analysis of mean fluorescence intensity (MFI) in 4T1 cells incubated with RB labeled m@BGLC at different time ($n = 3$). (D) Cellular uptake of BGLC and m@BGLC in 4T1, 3T3, CT26 and RAW264.7 cells after 4 h of incubation. Scale bar: 25 μm. (E) MFI statistical graph of different cells treated with m@BGLC ($n = 3$). (F) CLSM images, (G) flow cytometry histograms and (H) the corresponding MFI of DCF in 4T1 cells stained with DCFH-DA pre-incubated with BG, BGL, BGLC and m@BGLC ($n = 3$). Scale bar: 50 μm. (I) CLSM images and (J) the semi-quantitative analysis of MFI to evaluate the HClO production of 4T1 cells in different groups ($n = 3$). Scale bar: 50 μm. Data are expressed as the mean ± SD. $^{**}P < 0.01$, $^{***}P < 0.001$.

gen, time-dependent oxygen consumption process of nanozymes was monitored subsequently. As displayed in Fig. 2D, the oxygen consumption profiles of BG, BGL, BGLC, and m@BGLC were identical in glucose solution. In terms of oxygen consumption profiles in lactate solution, however, BG was shown to be entirely inactive due to the lack of LOx (Fig. 2E). In comparison, a similar downtrend was visible in BGL, BGLC and m@BGLC groups. Although the catalytic rates of these nanozymes were lower than that of free LOx, it could also exhaust oxygen in lactic acid solution within 900 s. Taken together, the prepared m@BGLC exhibited outstanding glucose and lactic acid catalytic abilities.

Biomimetic nanozymes can catalyze H_2O_2 into HClO with the assistance of CPO. Therefore, the catalytic performance of CPO in m@BGLC was evaluated using H_2O_2 content assay kit. Fig. 2F demonstrated that the BG and BGL groups produced a considerable amount of H_2O_2 and did not differ significantly from free GOx. Notably, BGL catalyzed the generation of H_2O_2 from lactate, but BG failed to produce H_2O_2 in lactate solution due to the lack of LOx (Fig. 2G). As expected, the BGLC and m@BGLC-treated groups had a much lower H_2O_2 generating ability in glucose and lactate solution, which should be attributed to the H_2O_2 consumption mediated by CPO. Subsequently, the catalysis activity of CPO in m@BGLC was measured using monochlorodimedon (MCD) indicator. Theoretically, CPO could convert MCD to dichlorodimedon (DCD) in the presence of KCl and H_2O_2. As demonstrated in Fig. 2H, the characteristic absorption of MCD dropped by 44% within 30 min in the m@BGLC mixture containing glucose and KCl, while it decreased by 26% in the m@BGLC mixture containing lactate and KCl. These experiments further demonstrated that m@BGLC could convert H_2O_2 into toxic HClO. In a word, m@BGLC inherited the original catalysis activities of GOx, LOx and CPO, which could efficiently consume both glucose and lactic acid with the production of HClO, making it a promising nanoplaform for tumor therapy (Fig. 2I).

The intracellular uptake of nanozymes was critical in cytotoxicity experiments. Thus, the cellular internalization of m@BGLC was primarily detected by confocal laser scanning microscopy (CLSM) and flow cytometry. First, m@BGLC were labeled with Rhodamine B (RB, red fluorescence) to observe cellular uptake. As shown in Figs. 3A–C, m@BGLC were internalized by 4T1 cells in a time-dependent manner. After 4 h of incubation with m@BGLC, the fluorescence intensity of 4T1 cells was about 6.26-fold higher than that of control group. Subsequently, the homologous targeting ability of m@BGLC was studied in a variety cell lines, including 4T1, 3T3, and CT26 cells. The fluorescence intensity of 4T1 cells treated with m@BGLC was 1.48-fold higher than that of the BGLC-treated group (Fig. 3D and Fig. S4 in Supporting information). It was worth noting that the cellular uptake of BGLC was 2.08-fold (for 3T3 cells) and 4.72-fold (for CT26 cells) higher than that of the same cell lines treated with m@BGLC (Fig. S4). Moreover, the uptake of m@BGLC by 4T1 cells was 3.48 and 4.91 times that of 3T3 and CT26 cells, respectively (Fig. 3E). These findings demonstrated that camouflaged m@BGLC exhibited superior selectivity to homologous 4T1 cells. To evaluate whether biomimetic nanozymes inherited the immune escape ability, m@BGLC and BGLC were respectively cultured with RAW264.7 cells to analyze the phagocytosis. It was a remarkable fact that RAW264.7 cells incubated with m@BGLC showed less red fluorescence than those cells treated with BGLC (Fig. 3D and Fig. S4). What is more, the uptake of m@BGLC by 4T1 cells was 4.60 times that of by RAW264.7 (Fig. 3E), implying that the presence of membrane proteins could inhibit macrophage cell uptake in reticuloendothelial system. Consequently, m@BGLC would successfully escape immune cell phagocytosis.

As a kind of ROS, HClO is one of the most powerful effectors of directly destroying proteins or nucleic acids. In this work, the

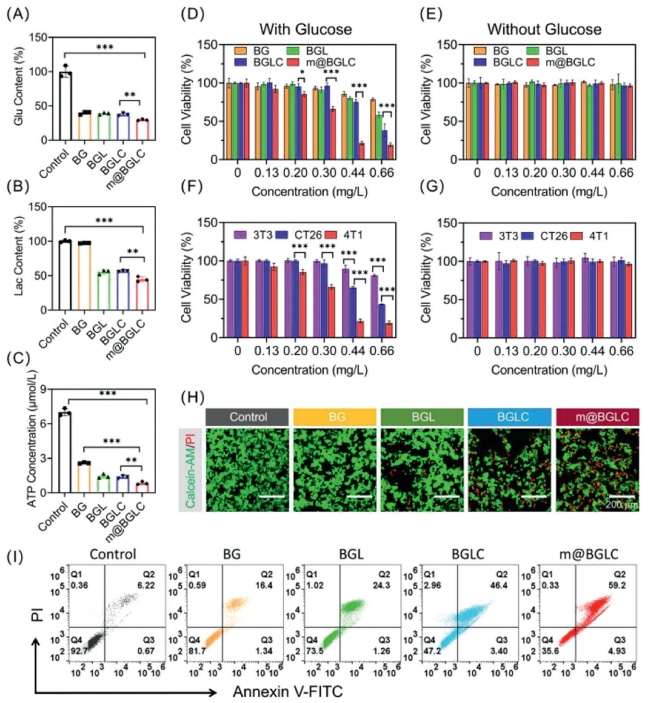

Fig. 4. *In vitro* nutrients deprivation and anti-tumor effect of m@BLGC. (A) Glucose concentration and (B) lactate concentration changes in 1640 medium after treatment with different nanozymes ($n = 3$). (C) Intracellular ATP reduction of 4T1 cells after treatment with different nanozymes ($n = 3$). Cytotoxicity of nanozymes to 4T1 cells (D) with or (E) without glucose ($n = 3$). Cell viability of 3T3, CT26 and 4T1 cells after m@BGLC treatment (F) under glucose or (G) without glucose condition ($n = 3$). (H) CLSM images of calcein-AM and propidium iodide (PI) co-stained 4T1 cells after incubation with different nanozymes. Scale bar: 200 μm. (I) Apoptosis analysis of 4T1 cells after incubation with BG, BGL, BGLC and m@BGLC. Data are expressed as the mean ± SD. $^{*}P < 0.05$, $^{**}P < 0.01$, $^{***}P < 0.001$. FITC, fluorescein isothiocyanate.

ROS generation ability of m@BGLC was firstly determined by using DCFH-DA indicator. Notably, in comparison to the poor green fluorescence of tumor cells treated with BG and BGL, BGLC-treated group displayed brighter green fluorescence (Fig. 3F), resulting from the production of HClO. Moreover, the green fluorescence of m@BGLC-treated group showed 1.14 times stronger than that of BGLC-treated group, which was attributable to the increased cellular uptake of m@BGCL for enhanced ROS generation (Figs. 3G and H). In addition, the green fluorescence intensity of the BGLC in 3T3 and CT26 cells was significantly higher than that of the m@BGLC, showing that the homologous targeting property of biomimetic nanozymes would reduce the nonspecific toxicity to other non-homologous cells (Fig. S5 in Supporting information). Furthermore, the capacity of m@BGLC to generate HClO was verified by using R6G hypochlorous acid as the specific sensor. As shown in Fig. 3I, there was distinctive red fluorescence in BGLC and m@BGLC groups. Furthermore, the semi-quantitative fluorescence analysis based on CLSM images proved that the excellent HClO producing ability of m@BGLC resulted in 1.24 times fluorescence increase compared to the BGLC-treated group (Fig. 3J). Moreover, the red fluorescence of BG and BGL groups was not significantly different from that of the control group, indicating that HClO could be only generated by CPO catalysis. These results showed that m@BGLC had attractive HClO production capability, which was critical in subsequent cytotoxicity experiments.

Next, the catalytic function of m@BGLC was measured in cell level. As shown in Fig. 4A, m@BGLC consumed more glucose than other groups, indicating that m@BGLC had a stronger capability to consume intracellular nutrients. Similarly, the m@BGLC-treated group had the lowest level of lactate (Fig. 4B), suggesting that it was capable of lactate deprivation. Because of the lack of LOx, the BG-treated group had an undetectable influence on the lactate concentration of the 4T1 cells. Furthermore, the intracellular ATP content following nanozymes treatment was evaluated to quantify the level of cellular metabolism (Fig. S6 in Supporting information). As expected, the lowest cellular ATP concentration was observed in the group of m@BGLC, suggesting its potential to ATP depletion (Fig. 4C).

Previous experiments demonstrated the outstanding catalytic function of nanozymes. After that, the toxicity of nanozymes against 4T1 cells was evaluated using MTT method with or without the presence of glucose. As displayed in Fig. 4D, cell viability was strongly dependent on nanozymes concentration. Furthermore, BGLC inhibited 4T1 cells more effectively than BG and BGL, demonstrating that synergistic starvation therapy and HClO-mediated oxidative damage could improve tumor therapy efficacy. Moreover, m@BGLC demonstrated greater inhibitory effect owing to its superior homologous targeting capacity. Because lactic acid was a glycolysis metabolite, the therapeutic effect of nanozymes was diminished in the absence of glucose (Fig. 4E). In addition, m@BGLC exhibited significantly higher cytotoxicity against 4T1 cells rather than other two cells (Fig. 4F). Furthermore, m@BGLC had lesser cytotoxicity than BGLC in CT26 and 3T3 cells, which highlighted a high tumor selectivity owing to its homologous targeting property (Fig. S7 in Supporting information). Similarly, the nanozymes were not detrimental in 3T3 and CT26 cells in the absence of glucose (Fig. 4G and Fig. S7). Moreover, the therapeutic efficacy was assessed using a live/dead cell staining method. As shown in Fig. 4H, m@BGLC showed the strongest cytotoxicity to homologous 4T1 cells, suggesting that the biomimetic nanozymes could produce considerable tumor killing effect. Finally, the cell death pathway of 4T1 cells induced by biominetic nanozymes was measured *via* flow cytometry. As reflected in Fig. 4I and Fig. S8 (Supporting information), the percentage of apoptosis cells was 18.27%, 26.88%, 49.81% and 66.98% after treatment with BG, BGL, BGLC and m@BGLC, respectively. In addition, as compared to BGLC, m@BGLC caused less apoptosis on CT26 and 3T3 cells (Fig. S9 in Supporting information). These results revealed the great advantage of m@BGLC for inducing tumor cell apoptosis by homologous targeting and cascade catalysis.

The hemolytic experiment was performed to evaluate the blood compatibility of biomimetic nanozymes prior to *in vivo* anticancer studies. All animal experiment protocols were approved by Southern Medical University's Institutional Animal Care and Use Committee. Fig. 5A showed that m@BGLC had minimal hemolysis (less than 5%) at doses ranging from 0.0625 g/L to 2 g/L, hinting an acceptable biocompatibility for drug delivery *in vivo*. Furthermore, the *in vivo* distribution of m@BGLC (labeled by RB) in 4T1-tumor bearing mice was studied at various time points to assess its targeting effect. As indicated in Fig. 5B, m@BGLC could efficiently accumulate in tumor sites, whereas BGLC had lesser distributions in tumor locations throughout the experiment period. For the fluorescence imaging of the *ex vivo* tissues, m@BGLC group had much higher fluorescence intensity on tumor tissue than BGLC group, indicating a superior tumor targeting performance of m@BGLC (Fig. S10 in Supporting information). Notably, the highest fluorescence signal was observed in the kidney, implying that the nanozymes could be degraded and metabolized out of the body.

Encouraged by the above results, the antitumor assay of biomimetic nanozymes was conducted in 4T1 tumor bearing BALB/c mice. When the tumor volume reached around 100 mm^3, BALB/c mice were randomly divided into five groups ($n = 6$): (1) control, (2) BG, (3) BGL, (4) BGLC, and (5) m@BGLC. As shown in Figs. 5C and D, the tumors in the control group grew very fast, whereas the BG and BGL groups exhibited a partial reduction in tumor volume, demonstrating that nanozyme-mediated glucose

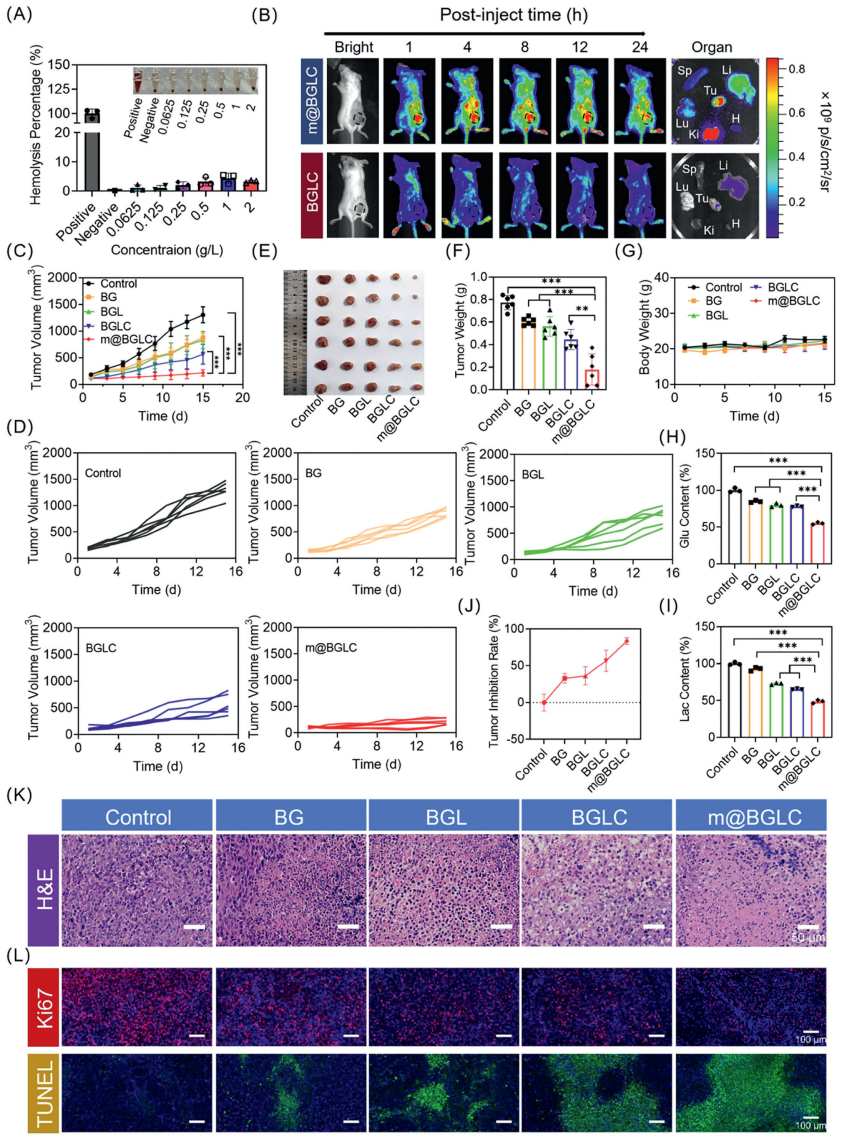

Fig. 5. *In vivo* biodistribution and tumor therapy of m@BGLC. (A) Hemolysis percentage of red blood cells after treatment with m@BGLC ($n = 3$). (B) *In vivo* fluorescence images of 4T1 tumor-bearing mice at different time points post intravenous injection with m@BGLC and BGLC as well as the corresponding *ex vivo* images of tissues after 24 h. H, Li, Sp, Lu, Ki and Tu represented heart, liver, spleen, lung, kidney and tumor tissues, respectively. (C) The average tumor volume in different groups during the treatment ($n = 6$). (D) Tumor growth curves of mice in 15 days after various treatments. (E) Photographs and (F) weight of tumors extracted from mice after different treatments for 15 days ($n = 6$). (G) Body weight changes of mice in different groups within 15 days ($n = 6$). (H) Tumor glucose content and (I) lactate concentration on the 15th day after different treatments ($n = 3$). (J) Tumor inhibition rate of different treatment groups ($n = 6$). (K) H&E (scale bar: 50 μm), (L) Ki67 and TUNEL staining photographs of tumor sections after different treatments. Scale bar: 100 μm. Data are expressed as the mean ± SD. $^{**}P < 0.01$, $^{***}P < 0.001$.

and lactate deprivation showed starvation therapy efficacy. Moreover, the tumor growth of BGLC group was much slower, indicating that combining starvation therapy and HClO-mediated oxidative damage was promising for tumor therapy. More excitingly, the m@BGLC demonstrated very attractive tumor ablation result with little tumor growth during the whole treatment (Figs. 5E and F), and the tumor inhibition rate was calculated to be 83.41% (Fig. 5J). Such excellent treatment efficacy could be due to its homologous targeting ability and amplified cascade catalysis efficiency. Importantly, all treatment groups showed no apparent weight loss during the experiment period (Fig. 5G), and hematoxylin-eosin (H&E) staining in the major organs of mice exhibited no obvious pathological damage (Fig. S11 in Supporting information), demonstrating that the nanozymes had a good biosafety for tumor therapy in spite of the inevitable aggregation in normal tissues.

To explore the underlying mechanism of synergetic therapy, the contents of glucose and lactic acid in tumor site were measured. As shown in Figs. 5H and I, the m@BGLC group consumed considerably more glucose and lactic acid than the other groups, indicating that m@BGLC could cut down the tumorigenic nutrition source. This was of great benefit to generate HClO by self-amplifying cascade catalytic reaction. In addition, H&E assay showed that, compared with control group, m@BGLC-treated tumor tissues exhibited enormous vacuolar regions and nucleolus concentrated (Fig. 5K). Meanwhile, terminal-deoxynucleoitidyl transferase mediated nick end labeling (TUNEL) and Ki67 assay revealed m@BGLC treatment dramatically increased tumor cell apoptosis (Fig. 5L and Fig. S12 in Supporting information). Finally, serum biochemical analysis was used to determine the liver and renal function of mice after the 15 days treatment. The index parameters of all treatment groups were within the normal reference ranges, showing that the biomimetic nanozymes were safe for *in vivo* application (Table S1 in Supporting information). Overall, these results demonstrated that biomimetic nanozyme-assisted starvation ther-

apy combined with HClO-mediated oxidative damage was highly effective for achieving superior tumor ablation and minimal side effects.

In summary, biomimetic nanozymes called m@BGLC were designed for catalytic tumor inhibition through nutrients deprivation and oxidative damage induction. First, the nanozymes were constructed by crosslinking GOx, LOx and CPO using a naturally occurring polymer BSA with low immunogenicity and high biocompatibility. Next, the obtained nanozymes were biomimetic functionalized using breast cancer cell membrane to prepare m@BGLC, which were endowed with homologous targeting and immune escape properties. The selective accumulation of m@BGLC on breast cancer improved the bioavailability of nanozymes and amplified their catalytic performance *in vivo*. Subsequently, the deprivation of tumorigenic nutrition source triggered tumor starvation therapy due to large consumption of glucose and lactate. Cascade catalysis produced HClO induced an oxidative damage of cells to synergistically inhibit tumor growth. Finally, *in vitro* and *in vivo* studies indicated that m@BGLC maximized the lethality on breast cancer cells while minimized the side reactions on normal cells. Notably, m@BGLC might have a promising application in tumor immunotherapy because of its superior glucose and lactate consumption. Collectively, this design of biomimetic nanozymes shed light on exploiting bio-derived drug delivery systems for clinical transformation in tumor combination therapy.

Declaration of competing interest

The authors declare that they have no known competing financial interests or personal relationships that could have appeared to influence the work reported in this paper.

CRediT authorship contribution statement

Yingtao Zhong: Conceptualization, Investigation, Methodology, Writing – original draft. **Ziwen Qiu:** Investigation, Methodology. **Yanmei Li:** Investigation. **Jiaqi Huang:** Investigation. **Zhenming Lu:** Investigation. **Renjiang Kong:** Investigation. **Ni Yan:** Investigation. **Hong Cheng:** Funding acquisition, Project administration, Supervision, Writing – review & editing.

Acknowledgments

We are grateful for the financial support of Guangdong Basic and Applied Basic Research Foundation (No. 2022B1515020095) and National Natural Science Foundation of China (No. 52073140).

Supplementary materials

Supplementary material associated with this article can be found, in the online version, at doi:10.1016/j.cclet.2024.109846.

References

[1] X. Li, Y. Yang, B. Zhang, et al., Signal Transduct. Target. Ther. 7 (2022) 305.
[2] B.I. Reinfeld, W.K. Rathmell, T.K. Kim, J.C. Rathmell, Cell Mol. Immunol. 19 (2021) 46–58.
[3] G.A. Brooks, Cell Metab. 27 (2018) 757–785.
[4] J. Chen, Y. Zhu, C. Wu, J. Shi, Chem. Soc. Rev. 52 (2023) 973–1000.
[5] P.K. Parida, M.M. Palencia, V. Nair, et al., Cell Metab. 34 (2022) 90–105.
[6] S. Kumagai, S. Koyama, K. Itahashi, et al., Cancer Cell 40 (2022) 201–218.
[7] L. Yang, D. Wang, H. Jia, et al., Adv. Mater. 35 (2023) e2301455.
[8] J.W. Wang, Q.W. Chen, G.F. Luo, et al., ACS Nano 15 (2021) 17870–17884.
[9] L.Y. Yu, P.W. Shueng, H.C. Chiu, et al., ACS Nano 17 (2023) 13158–13175.
[10] J. Yu, Z. Wei, Q. Li, et al., Adv. Sci. 8 (2021) 2101467.
[11] Y. Wu, W. Chen, C. Wang, D. Xing, Chin. Chem. Lett. 35 (2024) 109096.
[12] Y. Zhuang, S. Han, Y. Fang, H. Huang, J. Wu, Coord. Chem. Rev. 455 (2022) 214360.
[13] Q. Feng, Y. Hao, S. Yang, et al., Acta Pharm. Sin. B 13 (2023) 775–786.
[14] Y. Shan, Q. Ni, Q. Zhang, et al., Acta Pharm. Sin. B 12 (2022) 1825–1839.
[15] Y. Zhao, J. Liu, M. He, et al., ACS Nano 16 (2022) 12118–12133.
[16] F. Duan, W. Jin, T. Zhang, et al., Adv. Mater. 35 (2023) e2209765.
[17] S. Jiang, X. Chen, J. Lin, P. Huang, Adv. Mater. 35 (2023) e2207951.
[18] S. Zhang, Y. Zhang, Y. Feng, et al., Adv. Mater. 34 (2022) e2206851.
[19] Z. Tang, Z. Xu, X. Zhu, J. Zhang, Cancer Commun. 41 (2020) 16–36.
[20] R.W. Zhou, J. Xu, T.C. Martin, et al., Nat. Commun. 13 (2022) 6041.
[21] M. Wenes, A. Jaccard, T. Wyss, et al., Cell Metab. 34 (2022) 731–746.
[22] Q. Zhang, J. Wu, J. Wang, et al., Angew. Chem. Int. Ed. 59 (2020) 3732–3738.
[23] B. Liu, S. Liang, Z. Wang, et al., Adv. Mater. 33 (2021) e2101223.
[24] X. Zhang, L. Cheng, Y. Lu, et al., Nanomicro Lett. 14 (2021) 22.
[25] Y. Wang, D. Wang, Y. Zhang, et al., Bioact. Mater. 22 (2023) 239–253.
[26] X. You, L. Wang, J. Zhang, et al., Chin. Chem. Lett. 34 (2023) 107720.
[27] Y. Meng, S. Han, J. Yin, J. Wu, ACS Appl. Mater. Interfaces 15 (2023) 41743–41754.
[28] Y. Wang, C. Zhang, S. Han, et al., Chin. Chem. Lett. 35 (2024) 109578.
[29] M. Chen, Y. Sun, H. Liu, Interdiscip. Med. 1 (2023) e20220012.
[30] Y. Qu, B. Chu, X. Wei, et al., Adv. Mater. 34 (2022) e2107883.
[31] Z. Zhao, S. Dong, Y. Liu, et al., ACS Nano 16 (2022) 20400–20418.
[32] B. Geng, J. Hu, Y. Li, et al., Nat. Commun. 13 (2022) 5735.
[33] Y. Guo, Y. Fan, Z. Wang, et al., Adv. Mater. 34 (2022) e2206861.